Title

Assessing the zoonotic potential of a novel bat morbillivirus

Authors

Satoshi Ikegame[1], Jillian C. Carmichael[1], Heather Wells[2], Robert L. Furler O'Brien[3], Joshua A. Acklin[1], Hsin-Ping Chiu[1], Kasopefoluwa Y. Oguntuyo[1], Robert M. Cox[4], Aum R. Patel[1], Shreyas Kowdle[1], Christian S. Stevens[1], Miles Eckley[7], Shijun Zhan[7], Jean K. Lim[1], Ethan C. Veit[1], Matthew Evans[1], Takao Hashiguchi[5], Edison Durigon[6], Tony Schountz[7], Jonathan H. Epstein[8], Richard K. Plemper[4], Peter Daszak[8], Simon J. Anthony[9], Benhur Lee[1*]

Affiliations

1. Department of Microbiology at the Icahn School of Medicine at Mount Sinai, New York, NY 10029, USA.
2. Department of Ecology, Evolution and Environmental Biology, Columbia university, New York, NY 10027, USA.
3. Department of Medicine, Division of Infectious Diseases, Weill Cornell Medicine
4. Institute for Biomedical Sciences, Georgia State University, Atlanta, GA, USA
5. Laboratory of Medical virology, Institute for Life and Medical Sciences, Kyoto University, Kyoto 606-8507, Japan.
6. Departamento de Microbiologia, Instituto de Ciências Biomédicas, Universidade de São Paulo, Brazil.
7. Center for Vector-borne Infectious Diseases Department of Microbiology, Immunology and Pathology College of Veterinary Medicine Colorado State University.
8. EcoHealth Alliance, New York, NY 10018.
9. Department of Pathology, Microbiology, and Immunology, UC Davis School of Veterinary Medicine.

* Correspondence to: benhur.lee@mssm.edu and sjanthony@ucdavis.edu.

Competing interests: All authors declare no competing interests.

Keywords

measles virus, bats, morbillivirus, paramyxovirus, zoonosis, receptors

Abstract

Morbilliviruses are amongst the most contagious viral pathogens that infect mammals. Metagenomic surveys have identified numerous morbillivirus sequences in bats, but no full-length authentic morbillivirus has been isolated or characterized from bats. Here we detail the discovery of full-length Myotis Bat Morbillivirus (MBaMV) from a bat surveillance program in Brazil. After determining that MBaMV utilizes bat CD150 but not human CD150 as an entry receptor, we generated an infectious clone of MBaMV using reverse genetics. MBaMV exhibited features consistent with other morbilliviruses, including pleomorphic virions, P-editing and the rule-of-six. MBaMV replicated well in human epithelial cell lines in a nectin-4 dependent manner. Surprisingly, MBaMV was able to infect human macrophages in a CD150-independent manner. However, MBaMV was restricted by cross-neutralizing human sera and did not evade the human innate immune system, indicating that while zoonotic spillover into humans may be possible, MBaMV replication in humans would likely be restricted.

Introduction

Bats are significant reservoir hosts for many viruses with zoonotic potential[1]. SARS-CoV-2, Ebola virus, and Nipah virus are examples of such viruses that have caused deadly epidemics and pandemics when spilled over from bats into human and animal populations[2,3]. Careful surveillance of viruses in bats is critical for identifying potential zoonotic pathogens. However, metagenomic surveys in bats often do not result in full-length viral sequences that can be used to regenerate such viruses for targeted characterization[4], at least not without much further effort like 3' and 5' RACE. Improvements in sequencing technologies and bioinformatics have enabled more complete genome assemblies. Three metagenomic surveys published in the past year confirm that bats, and

55 to a lesser extent shrews and rodents, are hosts to diverse paramyxoviruses[5–7] that comprise
56 multiple genera (*Jeilongvirus*, *Morbillivirus*, *Henipavirus*). Metagenomic sequences, however
57 complete, cannot at present yield sufficiently accurate information about viral phenotypes in vitro
58 and in vivo. Detailed virological investigations are still needed to reify taxonomic discoveries.
59
60 Morbilliviruses are amongst the most contagious viral pathogens that infect mammals. While
61 numerous partial sequences of morbilliviruses have been identified in bats and rodents[4,5] in
62 metagenomic surveys, no full-length authentic morbillivirus has been isolated or characterized
63 from chiropteran hosts. The morbillivirus genus includes measles virus (MeV), canine distemper
64 virus (CDV), rinderpest virus, phocine distemper virus, cetacean morbillivirus, peste des petis
65 ruminants virus and feline morbillivirus[8]. A porcine morbillivirus was recently described to be the
66 putative cause of fetal death and encephalitis in pigs[9]. All morbilliviruses cause severe disease in
67 their natural hosts[10–14], and pathogenicity is largely determined by species specific expression of
68 canonical morbillivirus receptors, CD150/SLAMF1[15] and NECTIN4[16].
69
70 Here, we identify and characterize a novel morbillivirus from a vespertilionid bat species (*Myotis*
71 *riparius*) in Brazil, which we term myotis bat morbillivirus (MBaMV). MBaMV used *Myotis spp*
72 CD150 much better than human and dog CD150 in fusion assays. We confirmed this using live
73 MBaMV that was rescued by reverse genetics. Surprisingly, MBaMV replicated in primary human
74 myeloid but not lymphoid cells and did so in a CD150-independent fashion. This is in contrast to
75 MeV which is known to infect CD150+ human myeloid and lymphoid cells. Furthermore,
76 MBaMV replicated in human epithelial cells and used human nectin-4 almost as well as MeV.
77 Nonetheless, MBaMV P/V genes do not appear to antagonize human interferon induction and

signaling pathways and MBaMV was cross-neutralized, albeit to variable extents, by MMR vaccinee sera. Our results demonstrate the ability of MBaMV to infect and replicate in some human cells that are critical for MeV pathogenesis and transmission. Yet comprehensive evaluation of viral characteristics provide data for proper evaluation of its zoonotic potential.

Results

Isolation of MBaMV sequence. During a metagenomic genomic survey of viruses in bats, we identified a full-length morbillivirus sequence from a riparian myotis bat (*Myotis riparius*) in Brazil. This myotis bat morbillivirus (MBaMV) had a genome length of 15,720 nucleotides consistent with the rule of six and comprise of six transcriptional units encoding the canonical open reading frames (ORFs) of nucleo (N) protein, phospho (P) protein, matrix (M) protein, fusion (F) protein, receptor binding protein (RBP), and large (L) protein (Extended Data Fig. 1a). The sizes of these ORFs are comparable to their counterparts in the other morbilliviruses (Extended Data Fig. 1b). Phylogenetic analysis using the full-length L protein sequence indicated that MBaMV is most closely related to canine distemper virus (CDV) and phocine distemper virus (PDV) (Extended Data Fig. 1c, Extended Data Table 1).

Paramyxovirus proteins with the most frequent and direct interactions with host proteins, such as P and its accessory gene products (V and C) as well as the RBP, tend to exhibit the greatest diversity[17]. Morbillivirus P, V and C antagonize host-specific innate immune responses while its RBP interacts with host-specific receptors. That these proteins are under evolutionary pressure to interact with different host proteins is reflected in the lower conservation of MBaMV P/V/C (31-43%) and RBP (27-32%) with other morbillivirus homologs. This is in contrast to the relatively high conservation (52-76%) of MBaMV N, M, F, and L proteins with their respective morbillivirus

101 counterparts (Extended Data Fig. 2).

102

103 **Species specific receptor usage.** The use of CD150/SLAMF1 to enter myeloid and lymphoid cells
104 is a hallmark of morbilliviruses, and also a major determinant of pathogenicity. CD150 is highly
105 divergent across species, and accounts for the species restricted tropism of most morbilliviruses[18].
106 Thus, we first characterized the species-specific receptor tropism of MBaMV. We performed a
107 quantitative image-based fusion assay (QIFA) by co-transfecting expression vectors encoding
108 MBaMV-F and -RBP, along with CD150 from the indicated species into receptor-negative CHO
109 cells. MeV-RBP and F formed more syncytia in CHO cells upon human-CD150 (hCD150) co-
110 transfection compared to dog-CD150 (dCD150) or bat-CD150 (bCD150) (Fig. 1a, top row). In
111 contrast, MBaMV-RBP and F formed bigger and more numerous syncytia upon bCD150
112 overexpression than hCD150 or dCD150 (Fig. 1a, middle row). CDV-RBP and F formed extensive
113 syncytia with both dCD150 and bCD150, and moderate syncytia with hCD150 and even mock-
114 transfected cells (Fig. 1a, bottom row), suggesting a degree of promiscuity. We quantified these
115 differential syncytia formation results on an image cytometer as described[19] (Fig. 1b).
116 We also evaluated the receptor usage of MBaMV in a VSV-pseudotype entry assay. VSV-ΔG[Rluc]
117 bearing MeV-RBP and F entered hCD150-transfected CHO cells better than dCD150-, bCD150-,
118 or mock-transfected cells (Fig. 1c) as expected. MBaMV-pseudotypes entered only bCD150-
119 transfected CHO cells. CDV-pseudotypes showed good entry into dCD150- and bCD150-
120 transfected, but not hCD150-transfected CHO cells. These results are generally consistent with our
121 fusion assay results and support the species specificity of morbilliviruses. CDV has a high
122 propensity to cross species barriers and can cause disease in multiple carnivore families such as
123 large felids (e.g. lions, tigers), hyaenids (e.g. spotted hyenas), ailurids (e.g. red pandas), ursids (e.g.

124 black bears), procyonids (e.g. raccoons), mustelids (e.g. ferrets), viverrids (e.g. civets), and even
125 non-carnivore species such as javalinas (peccaries) and rodents (Asian marmots)[20]. CDV has also
126 been implicated in multiple outbreaks in non-human primates (various *Macaca* species)[21–23]. The
127 ability of CDV to use bCD150 and dCD150 with equal efficiency suggests potential for efficient
128 transmission from carnivores into some chiropteran species if other post-entry factors do not
129 present additional restrictions.
130
131 **Generation of MBaMV by reverse genetics.** Next, we attempted to generate a genomic cDNA
132 clone of MBaMV that we could rescue by reverse genetics. We synthesized and assembled the
133 putative MBaMV genome in increasingly larger fragments. Two silent mutations were introduced
134 in the N-terminal 1.5 kb of the L gene to disrupt a cryptic open reading frame in the minus strand
135 (Extended Data Fig. 3) that initially prevented cloning of the entire MBaMV genome. We
136 introduced an additional EGFP transcription unit at the 3' terminus and rescued this MBaMV-GFP
137 genome using the N, P, and L accessory plasmid from MeV (Extended Data Fig. 1a). MBaMV-
138 GFP was initially rescued in BSR-T7 cells but passaged, amplified, and titered on Vero-bCD150
139 cells (Extended Data Fig. 4a). MBaMV formed GFP-positive syncytia containing hundreds of
140 nuclei at 3 days post-infection (dpi) (Fig. 2a) and relatively homogenous plaques by 7 dpi (Fig.
141 2b). Transmission electron microscopy (TEM) (Fig. 2c) captured numerous virions budding from
142 Vero-bCD150 cells with pleiomorphic structure and size (~100-200 nm) consistent with
143 paramyxovirus particles. At high magnification, virions were outlined by protrusions suggestive
144 of surface glycoproteins. RNP-like structures can be found in the interior of the virion shown.
145 These observations are consistent with previous findings from MeV[24].
146

147 **Evaluation of receptor usage by MBaMV.** To understand how well CD150 from various hosts
148 supports MBaMV replication, we tested MBaMV growth in parental Vero-CCL81 cells and
149 isogenic derivatives constitutively expressing CD150 of human, dog, or bat. MBaMV formed huge
150 syncytia (Fig 3a) at 2 dpi in Vero-bCD150 cells and reached peak titers of ~10^5 PFU/ml at 3 dpi
151 (Fig 3b). MBaMV showed moderate syncytia spread and growth in Vero-dCD150 cells but peak
152 titers at 5 dpi was ~100-fold lower. No significant virus growth was detected in Vero or Vero-
153 hCD150 cells. These results confirm that MBaMV can use bCD150 but not hCD150 for efficient
154 cell entry and replication. MBaMV appears to use dCD150, albeit to a much lesser extent than
155 bCD150.
156 MeV uses human nectin-4 as the epithelial cell receptor[25,26] which mediates efficient virus
157 shedding from the affected host[16,27]. CDV also uses human nectin-4 efficiently for entry and
158 growth[23]. To test if MBaMV can use human nectin-4 in an epithelial cell context, we evaluated the
159 replication kinetics of MBaMV in human lung epithelial cells that express high (H441) or low
160 (A549) levels of nectin-4[16,28](Extended Data Fig. 4b). Surprisingly, MBaMV showed efficient
161 virus spread (Fig. 3c) in H441 cells and reached 10^4 PFU/ml by 6 dpi (Fig. 3d). In contrast,
162 MBaMV showed small GFP foci and 10 times lower titer in A549 cells. Comparing the Area Under
163 Curve (AUC) revealed significant differences in this growth curve metric (Fig. 3e). However, MeV
164 still replicated to higher titers than MBaMV in H441 cells (Fig. 3d-e). This could be due to species
165 specific host factors or differences in interferon antagonism between human and bat
166 morbilliviruses. Thus, we tested MBaMV versus MeV growth in interferon-defective Vero-human
167 nectin-4 cells (Vero-hN4). MBaMV and MeV replicated and spread equally well on Vero-hN4 cells
168 (Fig 3f-g), validating the ability of MBaMV to use human nectin-4, and suggesting that MBaMV
169 may not be able to counteract human innate immune responses.

170

171 **Molecular characterization of MBaMV.** To better understand the transcriptional profile of
172 MBaMV, we used Nanopore long-read direct RNA sequencing to sequence the mRNAs of
173 MBaMV-infected Vero-bCD150 cells at 2 dpi (MOI=0.01). We found a characteristic 3'- 5'
174 transcriptional gradient where GFP>N>P>M>F>RBP>L (Extended Data Fig. 5a).
175 Morbilliviruses have a conserved intergenic motif (CUU) between the gene end and gene start of
176 adjacent genes 'AAAA-CUU-AGG'. This intergenic motif was not immediately apparent in the
177 long complex M-F intergenic region of the assembled MBaMV genome. However, the high
178 coverage of this M-F intergenic region (M read-through transcripts) identified the M-F intergenic
179 motif as 'CGU' instead of 'CUU' (Extended Data Fig. 5b).
180 The P gene of morbilliviruses is known to generate the V or W genes through the insertion of one
181 or two guanines, respectively, at the conserved editing motif (AAAAGGG)[29], which is present in
182 MBaMV. Amplicon sequencing of the P gene editing motif—from the same mRNA pool used
183 above—revealed the frequency of P, V, and W mRNA is 42.1%, 51.2%, and 2.6%, respectively
184 (Extended Data Fig. 5c), suggesting that the major interferon antagonist (V) is produced. This P-
185 editing ratio is similar to what has been found in previous studies [30].
186 We next evaluated the expression and cleavage of two surface glycoproteins (RBP and F). C-
187 terminal AU-1 tagged F construct showed uncleaved F0 and cleaved F1 (Extended Data Fig. 5d).
188 C-terminal HA tagged RBP construct showed monomer in addition to oligomers (Extended Data
189 Fig. 5e). MBaMV-RBP showed smear above 110 kDa which is suggestive of oligomerization. This
190 oligomerization was also seen with MeV-RBP but not with CDV RBP suggesting differential
191 stability under the sub-reducing conditions used.
192

193 **Species tropism of MBaMV.** The two suborders of chiropterans (bats), Pteropodiformes
194 (Yinpterochioptera) and Vespertilioniformes (Yangochiroptera), include more than 1,400 species
195 grouped into 6 and 14 families, respectively[31]. Myotis bats belong to the prototypical
196 Vespertilionidae family that is the namesake of its suborder. Jamaican fruit bats (*Artibeus*
197 *jamaicensis*) belong to the same suborder as myotis bats, albeit from a different family
198 (Phyllostomidae). We inoculated 6 Jamaican fruit bats available in a captive colony via two
199 different routes with MBaMV to assess its pathogenicity *in vivo*. All bats remained asymptomatic
200 and showed no evidence of developing systemic disease up to 3 weeks post-infection. Nor could
201 we detect any molecular or serological evidence of productive infection (Extended Data Fig. 6).
202 Inspection of Jamaican fruit bat and myotis CD150 sequences revealed key differences in the
203 predicted contact surfaces with RBP (discussed below), which we speculate are responsible for the
204 species-specific restriction seen in our experimental challenge of Jamaican fruit bats with MBaMV.
205 To identify RBP-CD150 interactions likely involved in determining host species tropism, we
206 compared the amino acid sequences at the putative contact surfaces of morbillivirus RBPs and
207 their cognate CD150 receptors. Using PDBePISA[32], we identified three key regions in MeV-RBP
208 (residues 188-198, 498-507, and 524-556, Extended Data Fig. 7a-c) occluding two regions in
209 CD150 (residues 60-92 and 119-131 of human CD150, Extended Data Fig. 8) in the crystal
210 structure of MeV-RBP bound to CD150 (PDB ID: 3ALW)[33]. Alignment of key regions in
211 morbillivirus RBPs implicated in CD150 interactions reveals virus-specific differences that
212 suggest adaptation of morbillivirus RBPs to the CD150 receptors of their natural host. Most
213 notably, MBaMV lacks the DxD motif at residues 501-503 (505-507 in MeV) that is present in all
214 morbilliviruses except FeMV (Extended Data Fig. 7). These residues form multiple salt bridges
215 and hydrogen bonds that stabilize MeV-RBP and hCD150 interactions. Their conservation suggest

216 they perform similar roles for other morbilliviruses. On the CD150 side (Extended Data Fig. 8),
217 residues 70-76 and 119-126 are the most variable between host species. Interestingly, Jamaican
218 fruit bat and *Myotis* CD150 differ considerably in these regions, providing a rationale for the non-
219 productive infection we saw in our Jamaican fruit bat challenge experiments.
220

221 **Susceptibility of human myeloid and lymphoid cells to MBaMV.**

222 Alveolar macrophages and activated T- and B-cells expressing CD150 are the initial targets for
223 measles virus entry and systemic spread. To better assess the zoonotic potential of MBaMV, we
224 compared how well human and bat morbilliviruses can infect human monocyte-derived
225 macrophages (MDMs) and peripheral blood mononuclear cells (PBMCs). Both MeV and MBaMV
226 infected MDMs were clearly GFP+ 24 hpi (Fig. 4a), but infection was variable between donors
227 and even between different viral stocks on the same donor (Fig. 4b and 4d). However, MeV
228 infection of MDMs was inhibited by sCD150 whereas MBaMV infection was not (Fig. 4c). MDMs
229 had variable expression of CD150 (10-30% CD150+) but morbillivirus infection did not appear to
230 be correlated with CD150 expression (Fig. 4d). Conversely, when PBMCs were stimulated with
231 concanavalin A and IL-2, only MeV robustly infected these cells (Fig. 4e).
232

233 **MBaMV infection may be blocked by human immune defenses**

234 MeV-specific antibodies resulting from vaccination can provide cross protection against CDV
235 infection[34]. To assess if human sera from MeV-vaccinated individuals could contain cross-
236 neutralizing antibodies to MBaMV, we pooled MMR-reactive human sera and measured their
237 ability to neutralize MeV, MBaMV, and CDV in hCD150, bCD150, and dCD150-expressing Vero
238 cells. Human sera effectively neutralized MeV and MBaMV infection and, to a lesser extent, CDV

239 infection (Fig. 5a, left and center panels). Conversely, sera from CDV-infected ferrets neutralized
240 CDV infection much better than MeV or MBaMV (Fig. 5a, right panel). Sera from the MMR
241 groups 1 and 2 had higher IC50s for MeV and MBaMV than for CDV while CDV-specific sera
242 had a significantly higher IC50 for CDV than for MeV or MBaMV (Fig. 5b). These results indicate
243 that human sera contain cross-neutralizing antibodies for MBaMV.
244
245 The MeV proteins P and V interfere with the innate immune system by disrupting the IFN pathway.
246 Our sequencing results showed that MBaMV infection produced the P and V transcripts (Extended
247 Data Fig. 5c), so we sought to determine if the MBaMV P and V proteins could antagonize the
248 human IFN pathway. We found that cells transfected with MBaMV P or V and treated with IFN
249 did not block ISRE induction, unlike ZIKV NS5, which effectively counteracts the ISRE
250 (Extended Data Fig. 9a). Additionally, cells transfected with MBaMV P or V did not block the
251 induction of IFN when treated with RIG-I, MDA5, or MAVS (Extended Data Fig. 9b-d). These
252 data demonstrate that the MBaMV P and V proteins cannot antagonize the human IFN pathway.
253
254 **MBaMV is sensitive to morbillivirus RNA dependent RNA polymerase inhibitors**
255 Potential drug treatments are a critical issue for emerging viruses. Thus, we tested if MBaMV is
256 susceptible to currently available drugs. We have developed two orally bioavailable small
257 compounds targeting the L protein of morbilliviruses, GHP-88309[35] and ERDRP-0519[36]. The
258 differences between MeV and MBaMV across the five functional domains of the L protein are
259 shown schematically in Figure 6a[37]. *In silico* modelling (Fig. 6b) predicts that both drugs should
260 bind similarly to MeV and MBaMV L protein. Closer inspection of the ERDRP-0519 binding
261 pocket (Fig. 6c) shows 1155-1158 YGLE and H1288 residues interacting with ERDRP-0519.

262 These residues directly interact with ERDRP-0519 in MeV L[38]. Modeling of the GHP-88309
263 binding pocket (Fig. 6d) reveals involvement of E863, S869, Y942, I1009, and Y1105 residues
264 which were previously reported as escape mutants of GHP-88309 in MeV[35]. As predicted, both
265 drugs inhibited MBaMV growth in dose dependent manner (Fig. 6e and 6f). Although the EC_{50} of
266 GHP-88309 is lower for MeV than MBaMV, (0.6 μM and 3.0 μM, respectively), GHP-88309
267 reaches a plasma concentration of >30 μM in animal models, indicating this drug could be an
268 effective inhibitor of MBaMV *in vivo*.
269

270 **Discussion**

271 Metagenomic viral surveillance studies aided by next-generation sequencing have allowed
272 scientists to monitor viruses circulating in animal species and identify potential zoonotic threats[5–
273 7,39]. Surveillance of bat species has been particularly critical. For instance, >60 novel
274 paramyxovirus sequences were identified in a 2012 bat surveillance study, several of which
275 mapped to the *Morbillivirus* genus[4]. Recent metagenomic surveys confirm that bats harbor diverse
276 orthoparamyxoviruses [5–7]. While comparing novel virus sequences to known pathogens may help
277 inform the risks associated with future spillover events, this type of *in silico* modeling based on
278 viral sequences should also be complemented by functional characterization of such viruses. In
279 this study, we identified a full-length morbillivirus genomic sequence from *Myotis riparius* bats in
280 Brazil and generated an infectious virus clone using reverse genetics. With this approach, we
281 circumvented the arduous process of isolating and culturing live virus directly from animals and
282 instead produced MBaMV in the lab.

283 **MBaMV characterized as a morbillivirus**

284 Prior to this study, there were only 7 ICTV recognized morbilliviruses species, none of which were

285 isolated from bats. While the annotated MBaMV genome aligned with the classic morbillivirus
286 genome organization (N, P/V/C, M, F, RBP, and L), it was important to verify that virus generated
287 by reverse genetics successfully recapitulated morbillivirus biology. Fusion assays and entry
288 experiments confirmed that MBaMV preferentially used myotis CD150 over human or dog CD150
289 to enter transgenic Vero cells (Fig. 3), which fits the paradigm that CD150 is the major determinant
290 of host specificity for morbilliviruses. We also assessed P-editing—a hallmark of
291 paramyxoviruses—and found RNA editing of P-mRNA, creating V-mRNA (single G insertion) or
292 W-mRNA (double G insertion) of MBaMV. Interestingly, the proportion of V-mRNA at 51.2% of
293 total P transcripts is unusually high for orthoparamyxoviruses, resembling the now extinct
294 rinderpest virus (RPV) more than extant morbilliviruses[40].
295 In their natural hosts, morbillivirus are highly pathogenic and can cause deadly acute infections[41].
296 Thus, one reasonable prediction is that MBaMV would cause visible disease in the bat host.
297 However, when we challenged Jamaican fruit bats with MBaMV, we found the virus was *not* able
298 to cause systemic disease in the bats (Extended Data Fig. 6) and there was no evidence that
299 MBaMV productively infected these bats. This lack of infection could be due to the CD150
300 differences between the species—CD150 of Jamaican fruit bats and *Myotis* species is only 70%
301 conserved on the amino acid level (Extended Fig. 8). We predict that MBaMV infection is more
302 likely to cause serious disease in the *Myotis riparius* species. Alternatively, it is also possible that
303 bat morbilliviruses do not cause severe illness in their hosts since bats possess unique immune
304 systems that allow them to harbor deadly viruses such as Nipah, Ebola, and SARS without
305 exhibiting illness.[42]

306 **Zoonotic potential of MBaMV?**

307 When assessing the zoonotic potential of a novel virus, multiple factors must be considered,

308 including receptor usage, the existence of cross-neutralizing antibodies in human sera, and
309 interactions with the innate immune system. While non-human morbilliviruses are not currently
310 known to jump the species barrier and infect humans, we did find that MBaMV was able to utilize
311 human receptors *in vitro* to a certain extent. Traditionally, morbilliviruses use CD150 to enter
312 myeloid and lymphoid cells. However, unlike MeV which infects human macrophages via CD150,
313 MBaMV infects human macrophages in a CD150-independent manner (Fig. 4c)[43]. This result
314 indicates that a non-CD150/nectin-4 entry receptor for MBaMV exists on human macrophages. In
315 addition, MBaMV replicated well in H441 cells and in Vero cells expressing human nectin-4 (Fig.
316 3). CDV is also reported to use human nectin-4[23] and can replicate in H358 cells[44]. Alarmingly,
317 there have been several outbreaks of CDV in non-human primates, resulting in acute disease or
318 death in the animals[34]. In one outbreak, mutations were found in the RBP which rendered CDV-
319 RBP capable of efficiently using primate-CD150[23]. However, CDV is unlikely to adapt to humans
320 in the presence of cross-reactive MeV immunity. Human sera from MMR-vaccinated individuals
321 was able to cross-neutralize MBaMV infection *in vitro* (Fig. 5)—this would likely limit MBaMV
322 infection if MMR-vaccinated humans were exposed to the virus. Finally, while MeV P and V
323 proteins antagonize the innate immune response, MBaMV P and V were unable to block the IFN
324 induction or signaling (Extended Data Fig. 9). Taken together, our findings suggest that the
325 zoonotic potential for MBaMV is low due to cross-neutralizing anti-MeV antibodies and innate
326 immune restriction. The former reinforces the need to maintain broad and high coverage of
327 measles vaccination even when the virus has been eliminated in human populations.
328
329 In summary, our study provides a functional screening pipeline for evaluating the zoonotic
330 potential of a paramyxovirus identified only from metagenomic data. Our comprehensive

331 characterization will facilitate the screening of many other morbilliviruses present in bat and rodent
332 reservoirs, including at least one other full-length morbillivirus sequence present in the greater
333 spear-nosed bat (*Phyllostomus hastatus*). Given the deluge of metagenomic data from wild-life
334 surveillance studies, a formal blueprint for evaluating the zoonotic potential of paramyxoviruses
335 known to cause disease in humans is urgently needed.
336
337
338
339
340
341
342
343
344
345
346
347
348
349
350

351 **References**

352 1. Wang, L. F. & Anderson, D. E. Viruses in bats and potential spillover to animals and humans. *Curr. Opin.*
353 *Virol.* **34**, 79–89 (2019).
354 2. Han, H. J. *et al.* Bats as reservoirs of severe emerging infectious diseases. *Virus Res.* **205**, 1–6 (2015).

355 3. Letko, M., Seifert, S. N., Olival, K. J., Plowright, R. K. & Munster, V. J. Bat-borne virus diversity, spillover and
356 emergence. *Nat. Rev. Microbiol.* **18**, (2020).
357 4. Felix Drexler, J. *et al.* Bats host major mammalian paramyxoviruses. *Nat. Commun.* **3**, (2012).
358 5. Vanmechelen, B. *et al.* The characterization of multiple novel paramyxoviruses highlights the diverse nature
359 of the subfamily Orthoparamyxovirinae. *Virus Evol.* **8**, veac061 (2022).
360 6. Larsen Brendan B., Gryseels Sophie, Otto Hans W., & Worobey Michael. Evolution and Diversity of Bat and
361 Rodent Paramyxoviruses from North America. *J. Virol.* **96**, e01098-21 (2022).
362 7. Wells, H. L. *et al.* Classification of new morbillivirus and jeilongvirus sequences from bats sampled in Brazil
363 and Malaysia. *Arch. Virol.* (2022) doi:10.1007/s00705-022-05500-z.
364 8. Amarasinghe, G. K. *et al.* Taxonomy of the order Mononegavirales: update 2017. **162**, 2493–2504 (2017).
365 9. Arruda, B., Shen, H., Zheng, Y. & Li, G. Novel Morbillivirus as Putative Cause of Fetal Death and Encephalitis
366 among Swine. *Emerg. Infect. Dis.* **27**, 1858–1866 (2021).
367 10. Morens, D. M., Holmes, E. C., Davis, A. S. & Taubenberger, J. K. Global Rinderpest Eradication: Lessons
368 Learned and Why Humans Should Celebrate Too. *J. Infect. Dis.* **204**, 502 (2011).
369 11. Donduashvili, M. *et al.* Identification of Peste des Petits Ruminants Virus, Georgia, 2016. *Emerg. Infect. Dis.*
370 **24**, 1576 (2018).
371 12. Beineke, A., Puff, C., Seehusen, F. & Baumgärtner, W. Pathogenesis and immunopathology of systemic and
372 nervous canine distemper. *Vet. Immunol. Immunopathol.* **127**, 1–18 (2009).
373 13. Couacy-Hymann, E., Bodjo, C., Danho, T., Libeau, G. & Diallo, A. Evaluation of the virulence of some strains
374 of peste-des-petits-ruminants virus (PPRV) in experimentally infected West African dwarf goats. *Vet. J.* **173**,
375 178–183 (2007).
376 14. Bressem, M.-F. Van *et al.* Cetacean Morbillivirus: Current Knowledge and Future Directions. *Viruses* **6**, 5145
377 (2014).
378 15. Tatsuo, H., Ono, N., Tanaka, K. & Yanagi, Y. SLAM (CDw150) is a cellular receptor for measles virus. *Nature*
379 **406**, 893–897 (2000).

380 16. Mühlebach, M. *et al.* Adherens junction protein nectin-4 is the epithelial receptor for measles virus. *Nature*
381 **480**, 530–533 (2011).
382 17. Thibault, P. A., Watkinson, R. E., Moreira-Soto, A., Drexler, J. F. & Lee, B. Zoonotic potential of emerging
383 paramyxoviruses: knowns and unknowns. *Adv. Virus Res.* **98**, 1 (2017).
384 18. Ohishi, K., Maruyama, T., Seki, F. & Takeda, M. Marine Morbilliviruses: Diversity and Interaction with
385 Signaling Lymphocyte Activation Molecules. *Viruses* **11**, (2019).
386 19. Ikegame, S. *et al.* Fitness selection of hyperfusogenic measles virus F proteins associated with
387 neuropathogenic phenotypes. *Proc. Natl. Acad. Sci. U. S. A.* **118**, (2021).
388 20. Beineke, A., Baumgärtner, W. & Wohlsein, P. Cross-species transmission of canine distemper virus-an
389 update. *One Health Amst. Neth.* **1**, 49–59 (2015).
390 21. Yoshikawa, Y. *et al.* Natural infection with canine distemper virus in a Japanese monkey (Macaca fuscata).
391 *Vet. Microbiol.* **20**, 193–205 (1989).
392 22. Qiu, W. *et al.* Canine Distemper Outbreak in Rhesus Monkeys, China. *Emerg. Infect. Dis. J.* **17**, 1541 (2011).
393 23. Sakai, K. *et al.* Lethal canine distemper virus outbreak in cynomolgus monkeys in Japan in 2008. *J. Virol.* **87**,
394 1105–1114 (2013).
395 24. Nakai, M. & Imagawa, D. T. Electron Microscopy of Measles Virus Replication. *J. Virol.* **3**, 187 (1969).
396 25. Mateo, M., Navaratnarajah, C. K. & Cattaneo, R. Structural basis of efficient contagion: measles variations
397 on a theme by parainfluenza viruses. *Curr. Opin. Virol.* **0**, 16 (2014).
398 26. Lin, L. T. & Richardson, C. D. The host cell receptors for measles virus and their interaction with the viral
399 Hemagglutinin (H) Protein. *Viruses* **8**, 1–29 (2016).
400 27. Leonard, V. *et al.* Measles virus blind to its epithelial cell receptor remains virulent in rhesus monkeys but
401 cannot cross the airway epithelium and is not shed. *J. Clin. Invest.* **118**, (2008).
402 28. Noyce, R. S. *et al.* Tumor Cell Marker PVRL4 (Nectin 4) Is an Epithelial Cell Receptor for Measles Virus. *PLoS*
403 *Pathog.* **7**, (2011).
404 29. Cattaneo, R., Kaelin, K., Baczko, K. & Billeter, M. A. Measles virus editing provides an additional cysteine-

405 rich protein. *Cell* **56**, 759–764 (1989).

406 30. Wignall-Fleming, E. B. *et al.* Analysis of Paramyxovirus Transcription and Replication by High-Throughput
407 Sequencing. **93**, 1–17 (2019).

408 31. Eick, G. N., Jacobs, D. S. & Matthee, C. A. A nuclear DNA phylogenetic perspective on the evolution of
409 echolocation and historical biogeography of extant bats (Chiroptera). *Mol. Biol. Evol.* **22**, 1869–1886 (2005).

410 32. Krissinel, E. & Henrick, K. Inference of Macromolecular Assemblies from Crystalline State. *J. Mol. Biol.* **372**,
411 774–797 (2007).

412 33. Hashiguchi, T. *et al.* Structure of the measles virus hemagglutinin bound to its cellular receptor SLAM. *Nat.*
413 *Struct. Mol. Biol.* **18**, 135–142 (2011).

414 34. Kennedy, J. M. *et al.* Canine and Phocine Distemper Viruses : Species Barriers. *Viruses* **11**, (2019).

415 35. Cox, R. M. *et al.* Orally efficacious broad-spectrum allosteric inhibitor of paramyxovirus polymerase. *Nat.*
416 *Microbiol.* **5**, 1232–1246 (2020).

417 36. Krumm, S. A. *et al.* An orally available, small-molecule polymerase inhibitor shows efficacy against a lethal
418 morbillivirus infection in a large animal model. *Sci. Transl. Med.* **6**, 1–11 (2014).

419 37. Abdella, R., Aggarwal, M., Okura, T., Lamb, R. A. & He, Y. Structure of a paramyxovirus polymerase complex
420 reveals a unique methyltransferase-CTD conformation. *Proc. Natl. Acad. Sci. U. S. A.* **117**, 4931–4941
421 (2020).

422 38. Cox, R. M., Sourimant, J., Govindarajan, M., Natchus, M. G. & Plemper, R. K. Therapeutic targeting of
423 measles virus polymerase with ERDRP-0519 suppresses all RNA synthesis activity. *PLOS Pathog.* **17**,
424 e1009371 (2021).

425 39. Li, B. *et al.* Discovery of Bat Coronaviruses through Surveillance and Probe Capture-Based Next-Generation
426 Sequencing. *mSphere* **5**, (2020).

427 40. Douglas, J., Drummond, A. J. & Kingston, R. L. Evolutionary history of cotranscriptional editing in the
428 paramyxoviral phosphoprotein gene. *Virus Evol.* **7**, (2021).

429 41. De Vries, R. D., Paul Duprex, W. & De Swart, R. L. Morbillivirus infections: An introduction. *Viruses* **7**, 699–

430 706 (2015).

431 42. Banerjee, A. *et al.* Novel Insights Into Immune Systems of Bats . *Frontiers in Immunology* vol. 11 Preprint
432 at (2020).

433 43. Minagawa, H., Tanaka, K., Ono, N., Tatsuo, H. & Yanagi, Y. Induction of the measles virus receptor SLAM
434 (CD150) on monocytes. *J. Gen. Virol.* **82**, 2913–2917 (2001).

435 44. Otsuki, N. *et al.* The V Protein of Canine Distemper Virus Is Required for Virus Replication in Human
436 Epithelial Cells. *PLOS ONE* **8**, e82343 (2013).

437 45. Anthony, S. J. *et al.* Further evidence for bats as the evolutionary source of middle east respiratory
438 syndrome coronavirus. *mBio* **8**, 1–13 (2017).

439 46. Kumar, S., Stecher, G., Li, M., Knyaz, C. & Tamura, K. MEGA X: Molecular evolutionary genetics analysis
440 across computing platforms. *Mol. Biol. Evol.* **35**, 1547–1549 (2018).

441 47. Ono, N. *et al.* Measles Viruses on Throat Swabs from Measles Patients Use Signaling Lymphocytic Activation
442 Molecule (CDw150) but Not CD46 as a Cellular Receptor. *J. Virol.* **75**, 4399–4401 (2001).

443 48. Seki, F., Ono, N., Yamaguchi, R. & Yanagi, Y. Efficient Isolation of Wild Strains of Canine Distemper Virus in
444 Vero Cells Expressing Canine SLAM (CD150) and Their Adaptability to Marmoset B95a Cells. *J. Virol.* **77**,
445 9943–9950 (2003).

446 49. Tatsuo, H., Ono, N. & Yanagi, Y. Morbilliviruses Use Signaling Lymphocyte Activation Molecules (CD150) as
447 Cellular Receptors. *J. Virol.* **75**, 5842–5850 (2001).

448 50. Seki, F. *et al.* The SI Strain of Measles Virus Derived from a Patient with Subacute Sclerosing Panencephalitis
449 Possesses Typical Genome Alterations and Unique Amino Acid Changes That Modulate Receptor Specificity
450 and Reduce Membrane Fusion Activity. *J. Virol.* **85**, 11871 (2011).

451 51. von Messling, V., Zimmer, G., Herrler, G., Haas, L. & Cattaneo, R. The Hemagglutinin of Canine Distemper
452 Virus Determines Tropism and Cytopathogenicity. *J. Virol.* **75**, 6418–6427 (2001).

453 52. Beaty, S. M. *et al.* Efficient and Robust Paramyxoviridae Reverse Genetics Systems . *mSphere* **2**, (2017).

454 53. Oguntuyo, K. Y. *et al.* Quantifying absolute neutralization titers against SARS-CoV-2 by a standardized virus

455 neutralization assay allows for cross-cohort comparisons of COVID-19 sera. *mBio* **12**, 1–23 (2021).
456 54. Hashiguchi, T. *et al.* Crystal structure of measles virus hemagglutinin provides insight into effective
457 vaccines. *Proc. Natl. Acad. Sci. U. S. A.* **104**, 19535–19540 (2007).
458 55. Waterhouse, A. *et al.* SWISS-MODEL: Homology modelling of protein structures and complexes. *Nucleic*
459 *Acids Res.* **46**, W296–W303 (2018).
460 56. Madeira, F. *et al.* The EMBL-EBI search and sequence analysis tools APIs in 2019. *Nucleic Acids Res.* **47**,
461 W636–W641 (2019).
462 57. Pei, J. & Grishin, N. V. AL2CO: Calculation of positional conservation in a protein sequence alignment.
463 *Bioinformatics* **17**, 700–712 (2001).
464 58. Noda, T. *et al.* Importance of the 1+7 configuration of ribonucleoprotein complexes for influenza A virus
465 genome packaging. *Nat. Commun.* **9**, 1–10 (2018).
466
467
468
469
470
471
472
473
474
475
476
477
478
479 **Materials and methods**
480 **Method to isolate bat morbillivirus sequence**
481 The bat surveillance was conducted in the Amazon region of Brazil. The bat was a subadult male
482 (immature, but independent) and apparently healthy. Mitochondrial DNA profiling (MW554523
483 and MW557650) identified the bat as a riparian myotis (*Myotis riparius*). RNA was subjected to

484 NGS analysis, and viral genome (MW557651) was assembled from fastq read files (GSE166170).
485 The bat was captured by mist net, then oral, rectal, and urogenital swabs were all collected for
486 RNA extraction. Total nucleic acid (TNA) was extracted using the Roche MagNA Pure 96 platform
487 following the manufacturer's protocol, then TNA was DNase treated (DNase I; Ambion, Life
488 Technologies, Inc.) and reverse transcribed using SuperScript III (Invitrogen, Life Technologies,
489 Inc.) with random hexamer primers. The cDNA was treated with RNase H before second-strand
490 synthesis by Klenow fragment (3′ to 5′ exonuclease) (New England Biolabs), then the double-
491 stranded cDNA was sheared into average of 200 bps fragments using a Covaris focused
492 ultrasonicator E210. Sheared cDNA was deep sequenced using the Illumina HiSeq 2500 platform
493 and reads were bioinformatically de novo assembled using MEGAHIT v1.2.8 after quality control
494 steps and exclusion of host reads using Bowtie2 v2.3.5[45]. This method was same as previously
495 published. The virus was identified in the rectal swab. MBaMV was identified as part of a
496 metagenomic survey of bats sampled in Brazil and Malaysia. All the metadata associated with this
497 study, including the number and species of bats sampled can be found in Wells et al.[7]
498

499 **Generation of phylogenetic tree and conservation matrix table**

500 Amino acid sequences of L proteins were aligned by ClustalW, then the evolutionary history of L
501 proteins was inferred by Maximum Likelihood method with bootstrap test of 1,000 replicates. All
502 processes were done in MEGA X[46]. For conservation matrix table, amino acid sequences of each
503 gene were aligned by ClustalW, then the conservations were evaluated. The accession numbers
504 used for the alignment were summarized in Table S1.
505

506 **Cells**

507 293T cells (ACTT Ca# CRL-3216), A549 cells (ATCC Ca# CCL-185), Vero cells (ATCC Cat#
508 CCL-81, RRID:CVCL_0059), and BSR T7/5 cells (RRID:CVCL_RW96) were grown in in
509 Dulbecco's modified Eagle's medium (DMEM, ThermoFisher Scientific, USA) supplemented
510 with 10% fetal bovine serum (FBS, Atlanta Biologicals, USA) at 37°C. NCI-H441 cells (ATCC
511 Ca# HTB-174) were grown in RPMI 1640 medium (ThermoFisher Scientific, USA) with 10%
512 FBS. Vero-hCD150 (Vero-human SLAM) cells are Vero cells derivative which constitutively
513 express hCD150. Vero-dCD150 cells are Vero cells derivative which constitutively express HA-
514 dCD150. Vero-hCD150 cells[47] and Vero-dCD150 cells[48] were provided by Dr. Yanagi at Kyushu

515 University and maintained in DMEM with 10% FBS. Vero-bCD150 cells and Vero-human nectin-
516 4 cells were generated as written below and maintained in DMEM with 10% FBS. CHO cells were
517 grown in DMEM/F12 (1:1) medium (gibco) with 10% FBS.
518
519 **Plasmids**
520 We cloned the open reading frame of hCD150, dCD150, and bCD150 (from *Myostis brandtii* since
521 the CD150 sequence from *M. riparius* is unknown*)* into the pCAGGS vector cut by *Eco*RI (NEB)
522 and *Nhe*I-HF (NEB). We introduced HA tag-linker-Igk signal peptides (amino acids corresponding
523 to; MVLQTQVFISLLLWISGAYG-YPYDVPDYA-GAQPARSP) at the N-terminus of CD150s as
524 previously reported[49]. The sequence of hCD150, dCD150, bCD150 sequence were from
525 NP_003028.1, NP_001003084.1, and XP_014402801.1, respectively. We synthesized codon
526 optimized gene sequences at GeneArt Gene Synthesis (Invitrogen), generating pCAGGS-Igk-HA-
527 hCD150, pCAGGS-Igk-HA-dCD150, pCAGGS-Igk-HA-bCD150. We also generated pCAGGS-
528 Igk-HA-bCD150-P2A-Puro which additionally express puromycin resistant gene. For pCAGGS-
529 human nectin-4-P2A-puro, synthesized DNA by GeneArt Gene Synthesis (Invitrogen) was cloned
530 into pCAGGS.
531 The sequence of MBaMV RBP and F open reading frame were synthesized by GenScript. These
532 were cloned into pCAGGS vector cut by *Eco*RI and *Nhe*I-HF with adding HA tag (RBP gene) or
533 AU1 tag (F gene) in C-terminus, generating pCAGGS-MBaMV-RBP-HA, pCAGGS-MBaMV-F-
534 AU1.
535 For MeV RBP and F expressing plasmid, we amplified RBP and F sequence from p(+) MV323-
536 AcGFP with the addition of HA-tag and AU1-tag same as MBaMV-RBP and -F, creating
537 pCAGGS-MeV-RBP-HA, pCAGGS-MeV-F-AU1. For CDV RBP and F cloning, we amplified
538 RBP and F sequence from pCDV-5804P plasmid with the addition of HA-tag and AU1-tag,
539 creating pCAGGS-CDV-RBP-HA, pCAGGS-CDV-F-AU1.
540 Genome coding plasmids for MeV; (p(+) MV323-AcGFP) and CDV; pCDV-5804P were kindly
541 gifted from Dr. Makoto Takeda[50] and Dr. Veronica von Messling respectively[51]. We transferred the
542 MeV genome sequence into pEMC vector, adding an optimal T7 promotor, a hammer head
543 ribozyme, and we introduced an eGFP transcriptional unit at the head of the genome (pEMC-
544 IC323-eGFP), which is reported in the previous study[19].
545 For the generation of MBaMV genome coding plasmid, we synthesized pieces of DNA at 2000 -

546 6000 bps at Genscript with the addition of eGFP transcriptional unit at the head of genome (eGFP-
547 MBaMV). DNA fragments were assembled into pEMC vector one-by-one using in-fusion HD
548 cloning kit (Takara), generating pEMC-eGFP-MBaMV. The N-terminal 1.5 kb of the L gene was
549 initially unclonable. Sequence analysis revealed a putative 86 aa open reading frame (ORF-X) in
550 the complementary strand. Introduction of two point mutations in this region to disrupt ORF-X
551 without affecting the L amino acid sequence (Extended Data Fig. 4) finally enabled cloning of the
552 full-length genome suggesting that ORF-X was likely toxic in bacteria.
553
554 **Recovery of recombinant MBaMV and MeV from cDNA.**
555 For the recovery of recombinant MBaMV, 4×10^5 BSR-T7 cells were seeded in 6-well plates. The
556 next day, the indicated amounts (written below) of antigenomic construct, helper plasmids (-N, -P
557 and -L from measles virus), T7 construct, and LipofectamineLTX / PLUS reagent (Invitrogen)
558 were combined in 200 mL Opti-MEM (Invitrogen). After incubation at room temperature for 30
559 minutes, the DNA - Lipofectamine mixture was added dropwise onto cells. The cells were
560 incubated at 37°C for 24 hours. The cells containing P0 viruses were trypsinized and passed onto
561 Vero-bCD150 cells (2.0×10^6 cells / flask in one 75cm^2 flask). We collected supernatant 2 days after
562 overlay (P1 virus) and reamplified MBaMV in fresh Vero-bCD150 cells (> 2X T175 cm^2 flasks).
563 These passage 2 (P2) stocks were titerred, frozen down in aliquots, and used for all experiments.
564 The amount of measles plasmids used for rescue is reported in our previous study[52]: 5 mg
565 antigenomic construct, 1.2 mg T7-MeV-N, 1.2 mg T7-MeV-P, 0.4 mg T7-MeV-L, 3 mg of a
566 plasmid encoding a codon-optimized T7 polymerase, 5.8 mL PLUS reagent, and 9.3 mL
567 Lipofectamine LTX.
568 The rescue of MeV was done exactly same way as MBaMV rescue except that 5 mg of pEMC-
569 IC323eGFP was used for transfection and Vero-hCD150 cells were used for coculturing.
570
571 **Titration of viruses and plaque assay**
572 For MBaMV, a monolayer of Vero-bCD150 cells in 12 well was infected by 500 ml of serially
573 diluted samples for 1 hour, followed by medium replacement with methylcellulose containing
574 DMEM. 5 dpi, the number of GFP positive plaque was counted to determine titer. For the plaque
575 assay, infected Vero-bCD150 cells were incubated under methylcellulose containing DMEM for 7
576 days. Cells were then stained with 1% crystal violet and 1% neutral red sequentially. For MeV, we

577 used Vero-hCD150 cells and fixed the plates at 4dpi.

578

579 **Growth analysis**

580 2.0 x 10^5 cells / well were seeded in 12 well plate. Cells were infected by indicated titer of viruses
581 (MOI 0.01 or 0.5) for one hour, followed by replacement of fresh medium. Viruses were grown
582 for 5 days with medium change every day. Collected supernatants were used for titration.

583

584 **Generation of Vero-bCD150 cells and Vero-human nectin-4 cells.**

585 4.0 x 10^5 of VeroCCL81 cells were transfected with 2 mg of pCAGGS-Igk-HA-bCD150-P2A-
586 Puro with Lipofectamine 2000 (Invitrogen); cells were selected under 5 mg/ml of puromycin
587 (Gibco) until colonies were visible. Colonies were isolated independently and checked for HA
588 expression using FACS. Vero-human nectin-4 cells were generated by transfecting pCAGGS-
589 human nectin-4-P2A-Puro into VeroCCL81 cells, followed by 5 mg/ml of puromycin selection,
590 and clone isolation. Surface expression was checked by FACS.

591

592 **Generation of VSV-pseudotyped virus and entry assay.**

593 6 x 10^6 cells of 293T were seeded in a 10cm dish (pre-coated by poly-L-lysine (Sigma)) one day
594 before transfection. 12 mg of RBP plus 12 mg of F coding plasmid from MeV, CDV, or MBaMV
595 were transfected to cells by PEI MAX (polysciences). Vesicular stomatitis virus (VSV)-deltaG-
596 Gluc supplemented by G protein (VSVDG-G*) were infected at MOI = 10 for one hour at 8 hours
597 post plasmid transfection. Cells were washed with PBS three times and medium was maintained
598 with Opti-MEM for 48 hours. Supernatant was collected and ultra-centrifuged at 25,000 rpm x 2
599 hours and the pellet was re-suspended with 100ul of PBS[53]. For the quantification of pseudotyped
600 viral entry, CHO cells in 10cm dish were transfected with 24 mg of hCD150, dCD150, or bCD150
601 expressing plasmid with PEI MAX. CHO cells were passaged onto 96 well plates at 8 hours post
602 transfection The pseudotyped-VSV of MeV, CDV, or MBaMV were used to infect the CHO cells.
603 *Renilla* luciferase units (RLU) were measured by *Renilla* luciferase assay system (Promega) to
604 quantify the pseudotype virus entry into cells.

605

606 **Image based fusion assay.**

607 CHO cells were seeded at 50,000 cells in 48-well dish 24 hours before transfection. Cells were

608 transfected with 200 mg of pCAGSS-RBP-HA (of MeV/CDV/MBaMV), 200 mg of pCAGGS-F-
609 AU1(of MeV/CDV/MBaMV), pCAGGS-Igk-HA-CD150 (20 ng human, 5 ng dog, or 20 ng bat),
610 and 50 mg of pEGFP-C1 Lifeact-EGFP (purchased from Addgene) with 2.5 ml of
611 polyethylenimine max (polysciences). At 36 hours post transfection, cells were imaged with a
612 Celigo imaging cytometer (Nexcelom) with the GFP channel, and pictures were exported at the
613 resolution of 5 micrometer / pixel. The GFP-positive foci (single cell or syncytia) were analyzed
614 by ImageJ (developed by NIH), creating the profile of individual GFP-positive foci with size
615 information.
616 For the evaluation of syncytia size, we first filtered the GFP-positive foci with the size of >= 10
617 pixel^2, which is the median size of GFP area in the well of MeV-F plus LifeactGFP transfection to
618 exclude non-specific background noise. Then we calculated the frequency of syncytia which is
619 defined as the GFP counts of >= 100 pixel^2 (10 times of median size of single cells) / total GFP
620 counts of >= 10 pixel^2.
621
622 **Surface expression check of bCD150 in Vero-bCD150 cells and human nectin-4 in Vero-**
623 **human nectin-4 cells by FACS**
624 50,000 cells in a 96 well plate were dissociated with 10 μM EDTA in DPBS, followed by a 2%
625 FBS in DPBS block. Cells were treated with primary antibody for one hour at 4˚C, then washed
626 and treated by secondary antibody for one hour at 4˚C. Vero-bCD150 cells were examined with a
627 Guava® easyCyte™ Flow Cytometers (Luminex) for the detection of signal. Vero-human nectin-
628 4 cells were subjected to Attune NxT Flow Cytometer (ThermoFisher Scientific). For primary
629 antibody, mouse monoclonal nectin-4 antibody (clone N4.61, Millipore Sigma) and rabbit
630 polyclonal HA tag antibody (Novus biologicals) were used at appropriate concentration indicated
631 by the vendors. For secondary antibody, goat anti-rabbit IgG H&L Alexa Fluor® 647 (Abcam) and
632 goat anti-mouse IgG H&L Alexa Fluor® 647 (Abcam) were used appropriately. FlowJo was used
633 for analyzing FACS data and presentation.
634
635 **Soluble CD150 production and purification**
636 Production and purification of soluble CD150 is as previously reported[54]. Soluble CD150 is a
637 chimera comprising the human V (T25 to Y138) and mouse C2 domains (E140 to E239) + His6-
638 tag, which was cloned into pCA7 vector. The expression plasmid was transfected by using

639 polyethyleneimine, together with the plasmid encoding the SV40 large T antigen, into 90%
640 confluent HEK293S cells lacking N-acetylglucosaminyltransferase I (GnTI) activity. The cells
641 were cultured in DMEM (MP Biomedicals), supplemented with 10% FCS (Invitrogen), l-
642 glutamine, and nonessential amino acids (GIBCO). The concentration of FCS was lowered to 2%
643 after transfection. The His6-tagged protein was purified at 4 days post transfection from the culture
644 media by using the Ni2+-NTA affinity column and superdex 200 GL 10/300 gel filtration
645 chromatography (Amersham Biosciences). The pH of all buffers were adjusted to 8.0. Soluble
646 CD150 Fc fusion avitag was purchased from BPSbioscience, and reconstituted by PBS.
647

648 **Macrophage experiments**

649 CD14+ monocytes were isolated from leukopaks purchased from the New York Blood Bank using
650 the EasySep Human CD14 positive selection kit (StemCell #17858). For macrophage
651 differentiation, CD14+ monocytes were seeded at 10^6 cells/ml and cultured in R10 media (RPMI
652 supplemented with FBS, HEPES, L-glutamine, and pen/strep) with 50 ng/ml of GM-CSF (Sigma
653 Aldrich G5035) in a 37˚C incubator. Media and cytokines were replaced 3 days post seeding. At 6
654 days post seeding, macrophages were infected with either MeV or MBaMV at 100,000 IU
655 (infectious units) per 500,000 cells and were spinoculated at 1,200 rpm for 1 hour at room
656 temperature. Virus inoculum was removed and cells were incubated in R10 media with GM-CSF
657 at 37˚C. For imaging experiments, macrophages were fixed in 4% PFA at 30 hours post infection
658 (hpi), stained with DAPI, and fluorescent and bright field images were captured on the Cytation 3
659 plate reader. For flow cytometry experiments, infected macrophages were stained for viability at
660 24 hpi (LIVE/DEAD fixable stain kit from Invitrogen L34976), treated with human Fc block (BD
661 Biosciences), stained with antibodies against CD14 (eBioscience clone 61d3) and HLA-DR
662 (eBioscience clone LN3), fixed in 2% PFA, permeabilized with saponin, and stained for
663 intracellular CD68 (eBioscience clone Y1/82A) and CD150 (eBioscience). Soluble CD150
664 (1mg/ml) or CD150 Avi-tag (BPS Bioscience) were incubated with MeV or MBaMV for 15
665 minutes prior to infection for inhibition experiments. Stained macrophages were run through an
666 Attune NxT Flow Cytometer and data was analyzed using FlowJo software (v10).
667

668 **T cell experiments**

PBMCs were isolated from fresh blood donations obtained through the New York Blood Center using density centrifugation and a ficoll gradient. Isolated PBMCs were then resuspended in RPMI media (10% FBS, 1% L-Glutamine, 1% Penicillin-Streptomycin) and were stimulated for T-cell activation with Concanavalin-A (ConA) at 5 ug/ml for 72 hours. Following, cells were washed once with PBS and stimulated with 10 ng/ml of IL2 for 48 hours. Cells were subsequently infected at an MOI of 0.2 with MeV, BaMV or were mock infected in 12 well plates at 10^6 cells/ml. Cells were collected 24 hours post infection, stained with Invitrogen's LIVE/DEAD Fixable dead cell far red dye as per the manufacturer's protocol, and were analyzed for eGFP expression by flow cytometry with an Attune NxT Flow Cytometer. Analysis was completed using FCSExpress-7. A total of 2 donors were utilized for this analysis, with the data from donor 1 shown in Figure 4.

Western blot for RBP and F protein

1 x 10^6 of 293T cells were seeded on to collagen coated 6 well plate. 293T cells were transfected by 2 mg of pCAGGS, pCAGGS-MBaMV-RBP-HA, or pCAGGS-MBaMV-F-AU1 using polyethylenimine max (polysciences). Cells were washed with PBS, then lysed by RIPA buffer. Collected cytosolic proteins were run on 4 - 15% poly polyacrylamide gel (Bio-rad. #4561086) and transferred onto PVDF membrane (FisherScientific, #45-004-113), followed by primary antibody reaction and secondary antibody reaction. Rabbit polyclonal HA tag antibody (Novus biologicals, #NB600-363), rabbit polyclonal AU1 epitope antibody (Novus biologicals, #NB600-453) was used for primary antibody for HA and AU1 tag detection. Rabbit monoclonal antibody (Cell signaling technology, #2118) were chosen as primary antibody to detect GAPDH. Alexa Fluor 647-conjugated anti-rabbit antibody (Invitrogen, #A-21245) was used as secondary antibody appropriately. Image capturing were done by Chemidoc™ MP (Biorad).

Transcriptome analysis of MBaMV

4.0x10^5 Vero-bCD150 cells were infected by MBaMV at MOI = 0.01. Cytosolic RNA was collected by 500 ml of Trizol (Ambion) at 2 dpi. Collected cytosolic RNA was sequenced by direct RNA sequence by MinION (Oxford Nanopore Technologies) with some modifications in the protocol. First, we started library preparation from 3 mg of RNA. Second, we used SuperScript IV (Invitrogen) instead of SuperScript III. Sequencing was run for 48 hours by using R9.4 flow cells.

700 The fastq file was aligned to MBaMV genome sequence by minimap2 and coverage information
701 was extracted by IGVtools.
702
703 **Evaluation of P mRNA editing**
704 Infection and RNA extraction was same as above (transcriptome analysis). 1 ug RNA was reverse
705 transcribed by TetroRT (bioline) with poly-A primer, followed by PCR with primer set of Pedit-f
706 (sequence; GGGACCTGTTGCCCGTTTTA) and Pedit-r (sequence;
707 TGTCGGACCTCTTACTACTAGACT). Amplicons were processed by using NEBNext Ultra
708 DNA Library Prep kit following the manufacturer's recommendations (Illumina, San Diego, CA,
709 USA), and sequenced by Illumina MiSeq on a 2x250 paired-end configuration at GENEWIZ, Inc
710 (South Plainfield, NJ, USA). Base calling was conducted by the Illumina Control Software (HCS)
711 on the Illumina instrument. The paired-end fastq files were merged by BBTools. These merged
712 fastq files were aligned to the reference sequence using bowtie2, creating a SAM file, and we
713 counted the number of P-editing inserts.
714
715 **Neutralization Assay**
716 Vero-hCD150, Vero-dCD150, and Vero bCD150 cells were seeded in 96-well plates. Two groups
717 of pooled human sera from people who previously received the MMR vaccine (3 individuals per
718 pool) and sera from ferrets infected with CDV (courtesy of Richard Plemper) were heat-inactivated
719 for 30 minutes at 56˚C. Equal amounts of CDV, MeV, and MBaMV (20,000 IU/mL) were
720 incubated with serial dilutions of the heat-inactivated sera for 15 minutes at room temperature.
721 Virus and sera were then added to the Vero cells with the correct receptor and placed at 37˚C. At
722 20 hours post infection, the cells were imaged using a Celigo imaging cytometer (Nexelcom) with
723 the GFP channel. Exported images were analyzed using ImageJ to measure the extent of viral
724 infection by GFP+ area (MeV and MBaMV), or total GPF + counts (CDV). The % reduction in
725 infection was calculated by setting the level of infection in the no sera control wells to 100%. The
726 normalized data was plotted using GraphPad Prism and neutralization curves were generated using
727 non-linear regression with [inhibitor] vs. normalized response. IC50 values were calculated for
728 each replicate using a robust fit model. Five replicates were completed for the MeV and MBaMV
729 neutralization with the pooled human sera and 2 replicates were repeated with CDV and the ferret
730 sera.

731

732 **Interferon Induction and Response Assays**

733 For ISG induction assays, HEK 293T cells were transfected with plasmids coding for ISG54-ISRE-
734 FLuc, TK-RLuc, and either empty vector, MBaMV P, MVaMV V, or ZIKV MR766 NS5. At 24
735 hours post-transfection, the cells with treated with 100U of human IFNb (at 100U/mL). Cells were
736 lysed 24 hours after IFNb treatment and FLuc and RLuc expression was measured using the
737 Promega Dual luciferase assay. Data was calculated as a ratio of Fluc:RLuc to normalize for
738 transfection efficiency. Two independent experiments with 3 technical replicates were completed.
739 To measure the antagonism of IFN induction (IFNb promoter activation), HEK 293T cells were
740 transfected with plasmids coding for IFNb-FLuc, TK-RLuc, an IFN promoter stimulant (either
741 RIG-I, MDA5, or MAVS), and empty vector, MBaMV P, MBaMV V, or HCV NS3/4A (potential
742 IFN antagonists). At 24 hours post transfection, cells were lysed and FLuc and RLuc expression
743 was measured by Promega Dual luciferase assay. Data was calculated as a ratio of Fluc:RLuc to
744 normalize for transfection efficiency. Two independent experiments with 3 technical replicates
745 were completed. For statistical analysis, one-way ANOVA with Dunnett's multiple comparisons
746 were performed with Prism.

747

748 **Bat challenge experiment and evaluation of infection.**

749 Six Jamaican fruit bats (*Artibeus jamaicensis*) were inoculated with $2x10^5$ PFU MBaMV-eGFP;
750 three bats were intranasally (I.N.) and 3 bats were intraperitoneally (I.P.). At 1 week post virus
751 inoculation, bats were subjected to blood and serum collection, visually inspected for GFP
752 expression around the nares, oral cavity, and eyes by LED camera in each group (I.N. and I.P.). At
753 2 weeks post virus infection, blood, serum, and tissues (lung, spleen, and liver) were collected
754 from one bat in each group. At 3 weeks post virus infection, blood, serum, and tissues (lung, spleen,
755 and liver) were collected from one bat in each group.

756 Blood RNA was extracted by Trizol. RNA was reverse transcribed by Tetro cDNA synthesis kit
757 (Bioline) with the primer of 'GAGCAAAGACCCCAACGAGA' targeting MBaMV-GFP genome,
758 then the number of genomes was quantified by SensiFAST™ SYBR® & Fluorescein Kit (Bioline)
759 and CFX96 Touch Real-Time PCR Detection System (Biorad). The primer set for qPCR is
760 'GGGGTGCTATCAGAGGCATC' and 'TAGGACCCTTGGTACCGGAG'.

761 Virus neutralization assay was done as follows. Heat inactivated (56˚C x 30 minutes) bat serum

762 was serially diluted by 3 times (starting from 5 times dilution) and mixed with 2 x 10^4 PFU /ml of
763 MBaMV at 1: 1 ratio for 10 minutes at room temperature. 100 ml of mixture was applied to Vero-
764 batCD150 cells in 96 well. GFP foci were detected and counted by Celigo imaging cytometer
765 (Nexcelom). GFP counts of serum treated samples were normalized by no serum treated well.
766 Tissues were fixed with 10% buffered formalin and embedded with paraffin, then thin-sliced. GFP-
767 IHC was performed by using VENTANA DISCOVERY ULTRA. Rabbit monoclonal antibody
768 (Cell signaling technology, #2956) was used as a primary antibody, and OMNIMap anti-rabbit-
769 HRP (Roche, #760-4310) was used as a secondary antibody. The GFP signal was visualized by
770 using Discovery ChromoMap DAB kit (Roche, #760-2513). Tissues were counterstained with
771 hematoxylin to visualize the nuclei.
772

773 **In-silico docking**

774 In silico docking was performed with MOE 2018.1001 (Chemical Computing Group), as
775 previously described[38]. A homology model of MBaMV L was created based on the structural
776 coordinates of PIV5-L (PDB ID: 6V86) using the SWISS-MODEL homology modeling server[55].
777 Prior to docking, the model of the MBaMV L protein was protonated and energy minimized. An
778 induced-fit protocol using the Amber10 force field was implemented to dock ERDRP-0519 and
779 GHP-88309 into MBaMV L. For binding of ERDRP-0519, residues Y1155, G1156, L1157, E1158,
780 and H1288 and for binding of GHP-88309, residues E858, D863, D997, I1009, and Y1106 were
781 pre-selected as docking targets, which are predicted to line the docking sites of ERDRP-0519 and
782 GHP-88309, respectively, in MeV L. Top scoring docking poses were selected and aligned in
783 Pymol to the previously characterized in silico docking poses of the inhibitors to MeV L protein.
784 Sequence alignment of MBaMV and MeV L proteins was performed using Clustal Omega[56].
785 Conservation was scored using the AL2CO alignment conservation server[57].
786

787 **Transmission electron microscopy (TEM)**

788 Routine transmission electron microscopy processing was done as described . The Vero-bCD150
789 cells infected by MBaMV for 3 days were washed with phosphate-buffered saline and then fixed
790 with 2.5% glutaraldehyde in 0.1 M sodium cacodylate buffer (pH 7.4) on ice for 1 hour. The cells
791 were scraped off the 100 mm tissue culture treated petri dish and pelleted by low-speed
792 centrifugation (400g for 5 minutes). The pellet was fixed for 30 minutes with the same fixative

793 before secondary fixation with 2% osmium tetraoxide on ice for 1 hour. The cells were then stained
794 with 2% uranyl aqueous solution *en bloc* for 1 hour at room temperature, dehydrated with a series
795 of increasing ethanol gradients followed by propylene oxide treatment, and embedded in Embed
796 812 Resin mixture (Electron Microscopy Sciences). Blocks were cured for 48 h at 65°C and then
797 trimmed into 70 nm ultrathin sections using a diamond knife on a Leica Ultracut 6 and transferred
798 onto 200 mesh copper grids. Sections were counterstained with 2% uranyl acetate in 70% ethanol
799 for 3 min at room temperature and in lead citrate for 3 minutes at room temperature, and then
800 examined with a JEOL JSM 1400 transmission electron microscope equipped with two CCD
801 camera for digital image acquisition: Veleta 2K x 2K and Quemesa 11 megapixel (EMSIS,
802 Germany) operated at 100 kV.
803
804 **Ethics declaration.**
805 Animal study was performed following the Guide for the Care and Use of Laboratory Animals.
806 Animal experiment was approved by the Institutional Animal Care and Use Committee of
807 Colorado State University (protocol number 1090) in advance and conducted in compliance with
808 the Association for the Assessment and Accreditation of Laboratory Animal Care guidelines,
809 National Institutes of Health regulations, Colorado State University policy, and local, state and
810 federal laws. Archival CDV hyperimmune ferret sera were obtained from previous animal
811 experiments approved by the Institutional Animal Care and Use Committee of Georgia State
812 University (protocol number XXXX).
813
814 **Human subjects research**
815 Normal primary dendritic cells and macrophages used in this project were sourced from 'human
816 peripheral blood Leukopack, fresh' which is provided by the commercial provider New York Blood
817 center, inc. Leukapheresis was performed on normal donors using Institutional Review Board
818 (IRB)-approved consent forms and protocols by the vendor. The vendor holds the donor consents
819 and the legal authorization that should give permission for all research use. The vendor is not
820 involved in the study design and has no role in this project. Samples were deidentified by the
821 vender and provided to us. To protect the privacy of donors, the vendor doesn't disclose any donor
822 records. If used for research purposes only, the donor consent applies. Aliquots of pooled immune
823 sera were obtained from a previous anonymous serosurvey study that was qualified as Exemption

824 4 under NIH Exempt Human Subjects Research guidelines (Icahn School of Medicine at Mount
825 Sinai).
826
827 **Data and materials availability:**
828 The raw next generation sequencing results of bat surveillance, P gene editing, and transcriptome
829 by MinION are uploaded at NCBI GEO: GSE166170, GSE166158, and GSE166172,
830 respectively.
831
832 Assembled MBaMV sequence and pEMC-MBaMVeGFP sequence information are available at
833 MW557651 and MW553715, respectively. Cytochrome oxidase I host sequence and cytochrome
834 b host sequence of virus infected bat are available at MW554523 and MW557650. MeV genomic
835 cDNA coding plasmid (pEMC-IC323eGFP) sequence is available at NCBI Genbank:
836 MW401770.
837
838 **Authors contributions**
839 SI, SJA and BL conceived this study. SI conducted fusion assay, rescuing viruses, growth analysis,
840 RNA sequencing of transcriptome analysis, and generation of cell lines written in the study. RLF
841 conducted TEM imaging. JCC, JA, AP, and JL performed the macrophage and T cell experiments
842 and data analysis. KYO conducted VSV-pseudotype entry assay. RMC and PKP provided ERDRP-
843 0519 and GHP-88309 in addition to *in silico* modelling of MBaMV-L. HPC evaluated protein
844 production by Western blot. TH provided structure-guided insights into conservation of RBP and
845 CD150 binding as well as soluble human CD150 for inhibition assay. KYO and SK evaluated
846 surface expression of morbillivirus receptors. CSS evaluated P-mRNA editing frequency from
847 NGS data. TS, ME, SZ performed bat challenge experiment. ED conducted bat surveillance in
848 collaboration with JEE and PD. SJA and HW conducted NGS analysis of bat surveillance and
849 retrieved MBaMV sequences. ME and EV performed the IFN response and Induction experiments.
850 JEE, PD and SJA provided insights into viral ecology and zoonotic threats. BL supervised this

study. SI, JCC, SJA, and BL wrote the manuscript.

Acknowledgements

S.I. was supported by Fukuoka University's Clinical Hematology and Oncology Study Group (CHOT-SG). This study was supported in part by NIH grants AI123449 (B.L.), AI071002 (R.K.P and B.L.), AI149033 (B.L. and J.L.), AI140442 (T.S.), AI134768 (T.S.), and USAID PREDICT (S.J.A, J.H.E., P.D., E.D.). J.C.C. J.A.A., K.Y.O, A.P., C.S.S. acknowledge support from T32 AI07647. K.Y.O. was additionally supported by F31 (AI154739). J.A.A was additionally supported by F31 (HL149295). J.C.C. was additionally supported by F32 (HL158173). This work was also supported by Japan Agent for Medical Research and Development (AMED) Grant 20wm0325002h (T.H.), JSPS KAKENHI Grant Numbers 20H03497 (T.H.) and Joint Usage/Research Center program of Institute for Frontier Life and Medical Sciences, Kyoto University (S.I.).

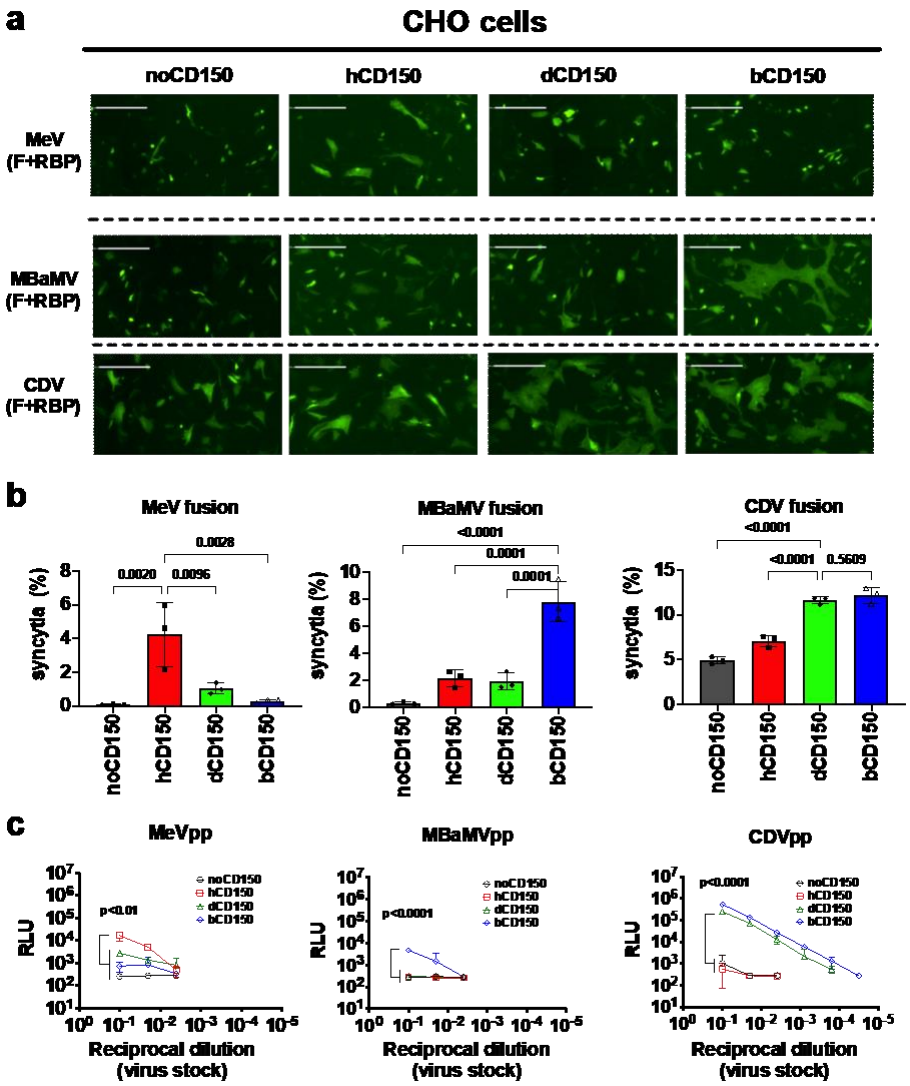

Figure 1. MBaMV envelope glycoproteins use host specific CD150 (SLAMF1) for fusion and entry. a, Syncytia formation in CHO cells co-transfected with the indicated morbillivirus envelope glycoproteins, species-specific CD150, and Life-act-GFP. Images were taken by the Celigo Imaging Cytometer (Nexcelom) at 48 hours post-transfection (hpt) and are computational composites from an identical number of fields in each well. White bar equals 200 µm. Brightness and contrast settings were identical. **b,** Quantification of syncytia formation in (a). Data are mean +/- S.D. from 3 independent experiments. Indicated adjusted p values are from ordinary one-way ANOVA with Dunnett's multiple comparisons test. **c,** VSV-pseudo particle (pp) entry assay showed similar trends. Adjusted p values obtained as in **(b)** but only for comparing groups at the highest viral inoculum used (10^{-1} reciprocal dilution).

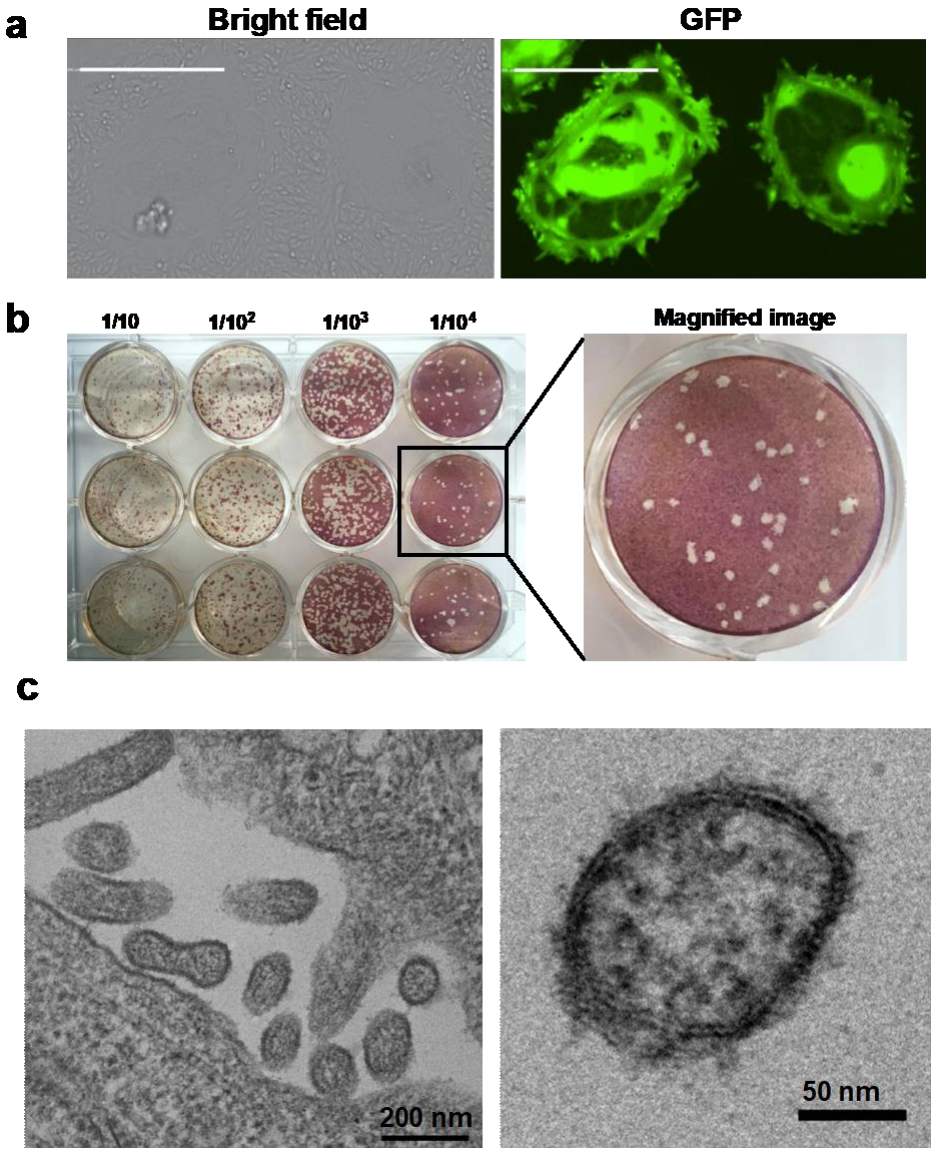

877
878
879 **Figure 2. Virological characterization of myotis bat morbillivirus (MBaMV). a,** Syncytia
880 formation in Vero-bCD150 cells induced by MBaMV 3 days post-infection (dpi). Cells formed
881 syncytia involving > 100 nuclei upon infection (bright field), which is clearly outlined by virus
882 expressed GFP (right). Scale bar equals 500 micrometers. **b,** MBaMV plaque formation in Vero-
883 bCD150 cells. Cells were infected by 10-fold serially diluted virus stock, incubated with
884 methylcellulose containing-DMEM and stained with crystal violet and neutral red 7 dpi. Diameter
885 of well is 22 mm. One well is magnified to show the plaque morphology in detail. **c,** shows
886 transmission electron microscopy (TEM) images of MBaMV virion on the surface of Vero-
887 bCD150 cells at 3 dpi. Numerous enveloped virions are budding from the plasma membrane (left).
888 Magnified image (right) shows virion and ribonucleoprotein complex (RNP).

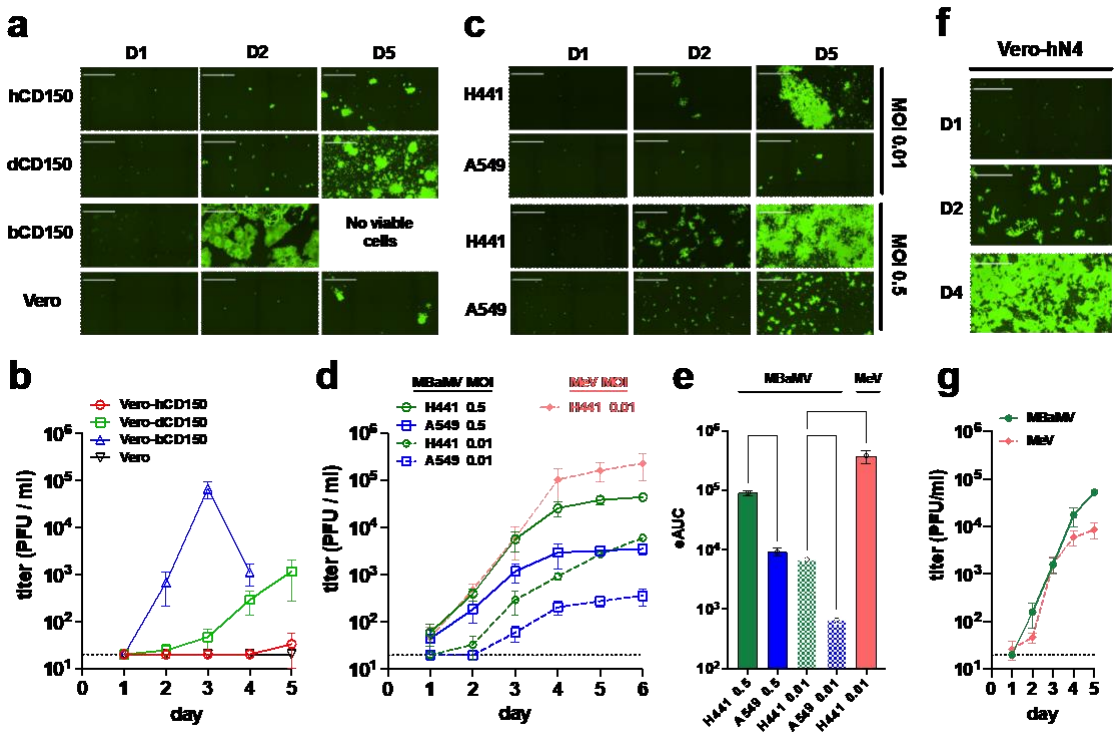

Figure 3. MBaMV replicates efficiently in cells expressing bCD150 and human nectin-4. a-b, Vero-hCD150, Vero-dCD150, Vero-bCD150, and Vero cells were infected with rMBaMV-EGFP (MOI 0.01). Virus replication and spread were monitored by imaging cytometry **(a)** and virus titer in the supernatant **(b)**. **a,** Large syncytia were evident in Vero-bCD150 cells by 2 dpi. **b,** Supernatant was collected every day and the virus titer was determined by a GFP plaque assay (see methods). Data shown are mean +/- S.D. from triplicate experiments. **c-e,** H441 and A549 cells were infected with rMBaMV-EGFP at a low (0.01) or high (0.5) MOI. Virus replication and spread were monitored as in **a-b**. **c,** Infected H441 and A549 cells at 1, 2 and 5 dpi (D1, D2, D5). **d,** Virus growth curves represented by daily titers in the indicated conditions. Data shown are mean titers +/- S.D. from triplicate infections. **e,** The empirical Area Under Curve (eAUC) was obtained from each growth curve and plotted as a bar graph (mean +/- S.D.) (PRISM v 9.0). Adjusted p values are indicated (one-way ANOVA Dunnett's T3 multiple comparison test). **f-g**, Vero-human nectin-4 cells (Vero-N4) were infected with MBaMV and MeV (MOI 0.01). **f,** MBaMV infected Vero-hN4 at D1, D2 and D4. **g,** Replicative virus titers for MBaMV and MeV on Vero-hN4 cells over 5 days (mean +/- S.D., n=3). White bar in **a, c,** and **f** equals 1 millimeter. All images shown are captured by a Celigo Imaging Cytometer (Nexcelom). Images are computational composites from an identical number of fields in each well. The limit of detection for virus titer determination is 20 PFU/ml and is indicated by the dotted line in **b, d, and g**.

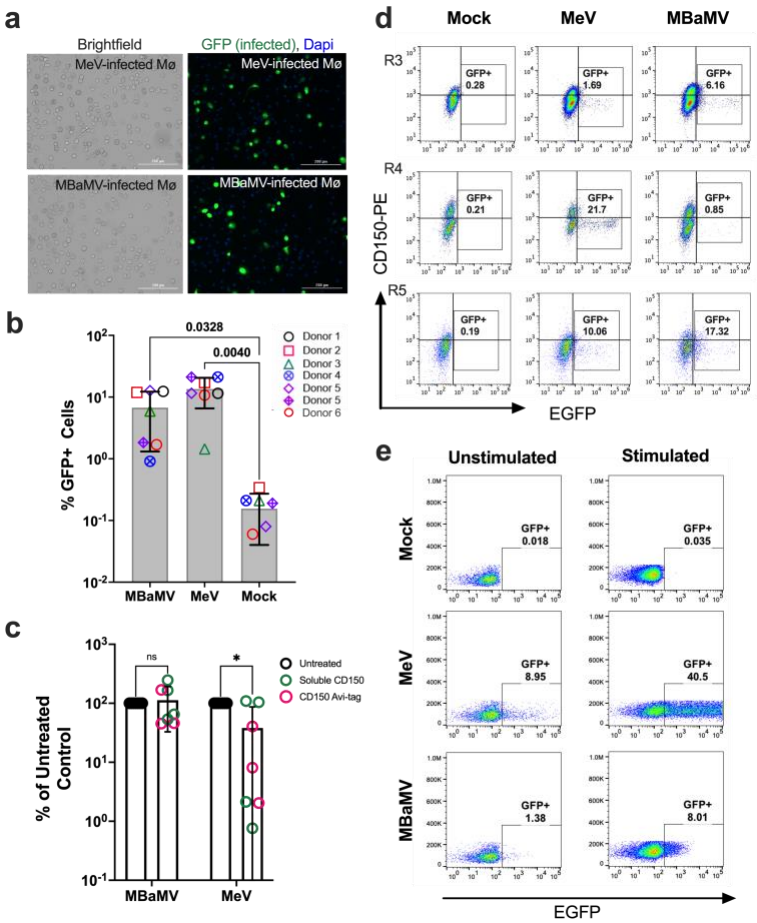

Figure 4. MBaMV infects human monocyte-derived macrophages (MDM) in a CD150-independent manner. a-b, MDMs were infected with MV323-EGFP or MBaMV ($1x10^5$ IU/sample) and were either **(a)** fixed by 2% PFA at 24 hpi, DAPI-stained and imaged (scale bar is 200 µm), or **(b)** quantified by flow cytometry. The percent of CD68+GFP+ MDMs from 6 donors are shown. Open and crossed symbols indicate experiments using lot 1 and lot 2 viruses, respectively. Adjusted p values are from one way ANOVA with Dunnett's multiple comparisons test. **c,** Soluble human CD150 (sCD150) or a CD150 Avi-tag inhibited MeV but not MBaMV infection of macrophages. GFP+ events in untreated controls were set to 100%, and entry under sCD150/ CD150 Avi-tag were normalized to untreated controls. Adjusted p values are from two-way ANOVA with Šídák's multiple comparisons test. In (**b**) and (**c**), data shown are mean +/- S.D. from multiple experiments (N=5-7) with individual values also shown. **(d)** Exemplar FACS plots from the summary data shown in (**b**) for CD150 staining. **e,** ConA/IL-2 stimulated PBMCs were infected with MeV or MBaMV (MOI of 0.1) and analyzed for GFP expression by flow cytometry at 24 hpi.

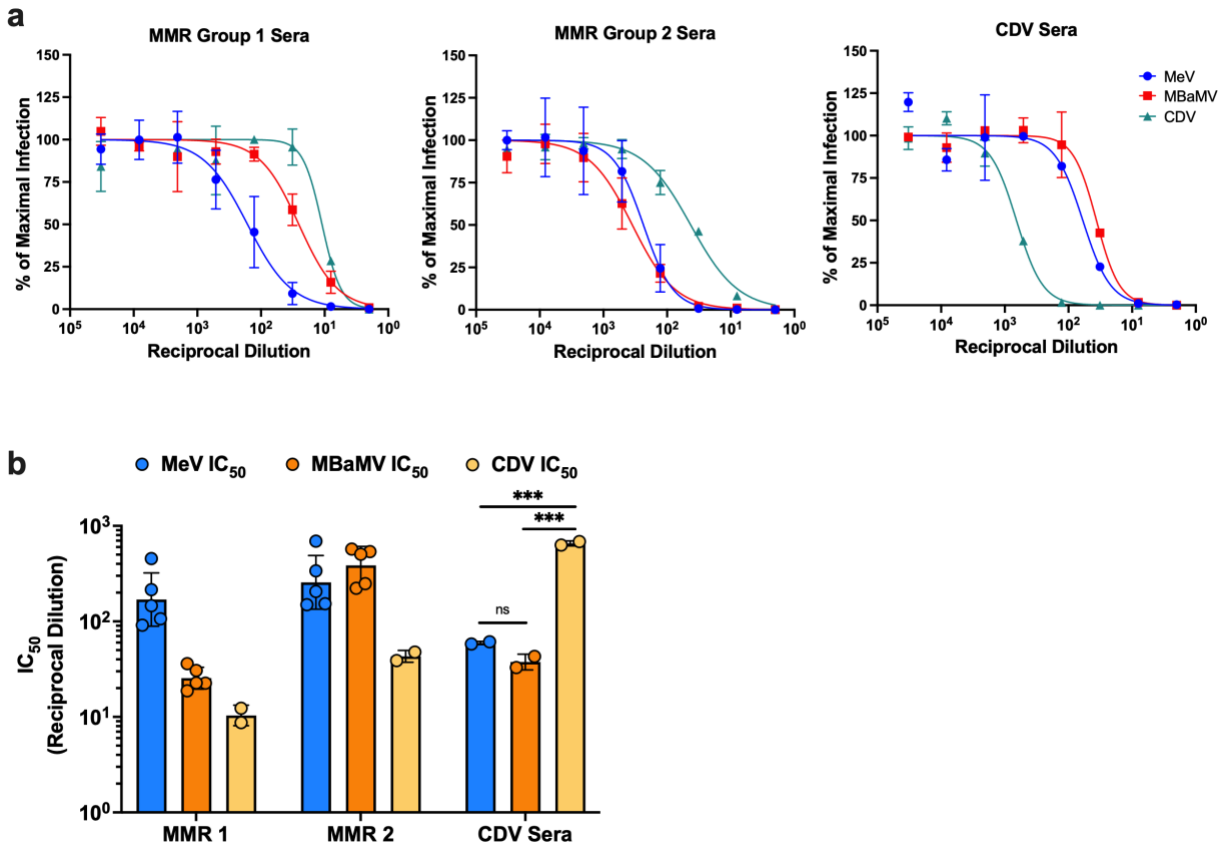

Figure 5. Human sera contains antibodies that partially cross-neutralize MBaMV. a) MeV, MBaMV, and CDV were incubated with serial dilutions of pooled human sera from MMR-vaccinated individuals (MMR group 1 and group 2) and sera from ferrets infected with CDV. The capacity for sera-treated virus to infect Vero cells expressing the appropriate receptor was measured by imaging infected cells 20 hpi, measuring the area of GFP+ cells, and calculating the reduction in infection compared to no sera controls. Neutralization curves were plotted for each virus and corresponding sera group. **b)** The IC50s from the neutralization curves shown in **a)** were generated for each replicate using a robust fit model and were plotted.

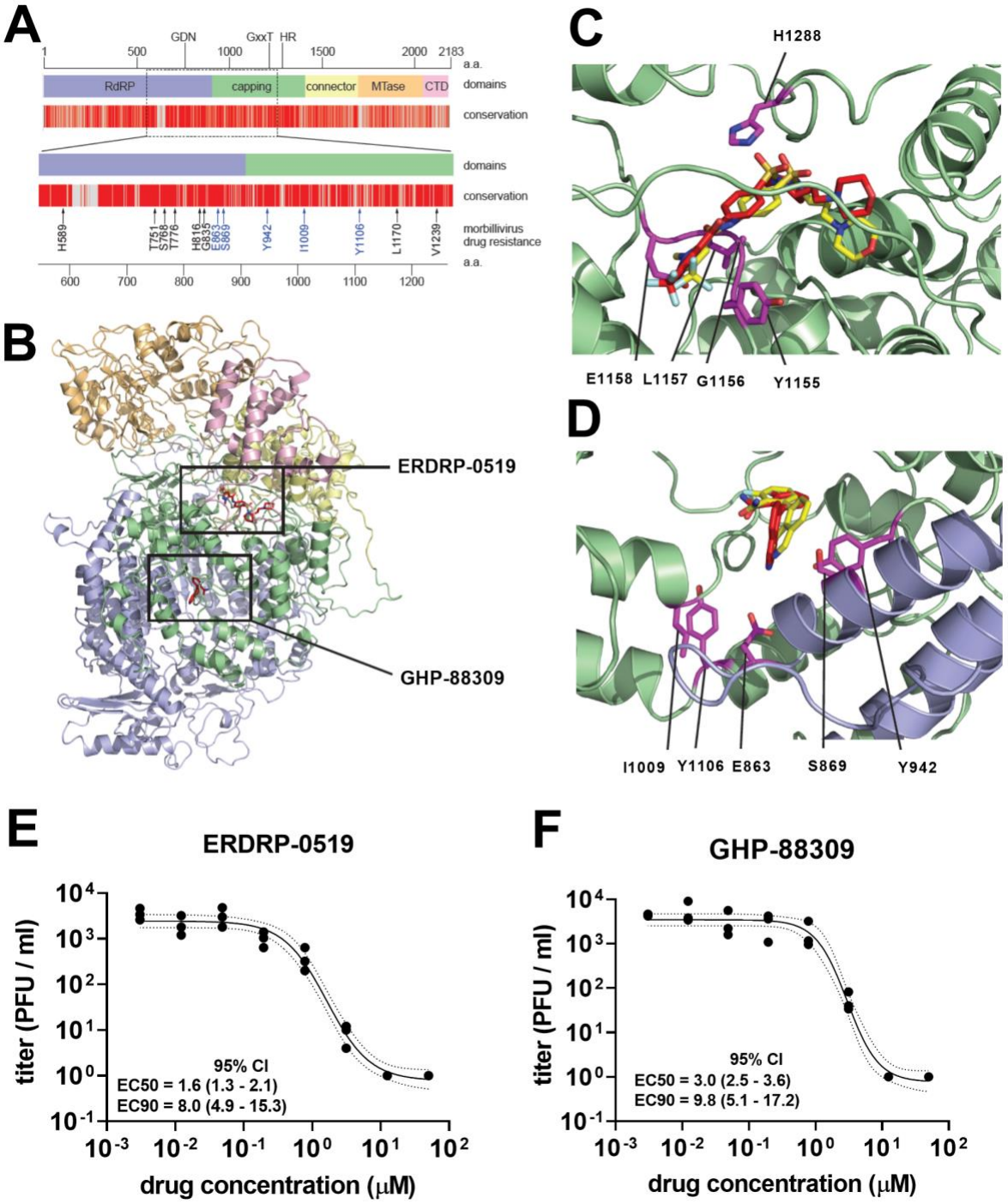

Figure 6. MBaMV is susceptible to RNA-dependent RNA polymerase inhibitor of ERDRP-0519 and GHP-88309. a, 2D-schematic of MBaMV L protein showing the layout of each domain. Conservation between the MeV and MBaMV L protein is shown. Differences between the MeV and MBaMV L proteins are shown as grey lines. b, A 3-D homology model of the

MBaMV L protein was generated using the structural coordinates of the PIV5 L protein (PDB ID: 6V86). The RNA-dependent RNA polymerase (RdRP), capping, connector, methyltransferase (MTase), and C-terminal (CTD) domains are colored blue, green, yellow, orange, and pink, respectively. The locations of the top scoring in silico docking poses for ERDRP-0519 and GHP-88309 are boxed and the compounds are shown as red sticks. c, The top scoring docking pose of ERDRP-0519 in the homology model of MBaMV L protein (red sticks). An overlay of the previously identified docking pose of ERDRP-0519 in a homology model of MeV L protein is shown (yellow sticks) (Cox et al, PLoS Pathog, 2021. PMID:33621266). Residues identified in previous photoaffinity crosslinking experiments (Y1155, G1156, L1157 and E1158) and H1288 of the HR motif are shown as magenta sticks. d, The top scoring docking pose of GHP-88309 in the homology model of MBaMV L protein (red sticks). An overlay of the previously identified docking pose of GHP-88309 in a homology model of the MeV L protein is shown (yellow sticks) (Cox et al, Nature Microbiol, 2020, PMID:32661315). Residues identified in MeV resistance profiling studies are shown as magenta sticks. e, shows the dose-response inhibition growth curves of ERDRP-0519 against MBaMV. Vero-bCD150 cells were infected by MBaMV at MOI = 0.01 for 1 hour, then inoculum was replaced by fresh media containing inhibitor at the indicated concentrations (0 to 50 micromolar). 2 dpi, viral supernatants were collected and tittered on Vero-bCD150 cells as described in methods. Dots represent the values from 3 independent experiments. Regression curve (solid line) and 95% CI (dot line) were generated in PRISM (v.8.0). f, shows the drug response of GHP-88309 against MBaMV growth. The virus inhibition was conducted identically as for ERDRP0519.